ATLAS DETECTOR SYSTEM — SELECTED TOPICS*

Piotr Malecki

H. Niewodniczański Institute of Nuclear Physics
Kawiory 26a, 30-055 Kraków, Poland

(Received November 4, 1999)

Overview of the ATLAS magnet system and transition radiation tracker is presented.

PACS numbers: 29.40.Gx

1. Introduction

ATLAS is designed and constructed as a general purpose pp experiment at the Large Hadron Collider at CERN. It is the project of the ATLAS Collaboration of about 1700 physicists and engineers from 144 universities and research institutes.

Its high discovery potential in large range of interesting physics questions has already been shown many times. It requires superb detector performance even at highest luminosities and energies delivered by the LHC. Results of many years of thorough detector and physics simulations and analyses have recently been collected in [1]. They are also summarized in another contribution to this School [2].

In addition, ATLAS (and CMS, another general purpose proton-proton experiment at LHC) assure precision measurements in many physics channels what will significantly improve results obtained by 2005 at other machines [3].

Such precision measurements depend on many experimental concepts and technical perfections. In this short lecture for the School of Theoretical Physics I will concentrate on two detector aspects of the ATLAS experiment which contribute significantly to the overall detector performance and which also make ATLAS very distinct from other "typical" collider detectors. An exceptional solutions for ATLAS magnet system and the transition radiation tracker — part of the inner detector — will be characterized.

* Presented at the XXXIX Cracow School of Theoretical Physics, Zakopane, Poland, May 29–June 8, 1999.

2. ATLAS Magnet System

ATLAS, the acronym for**A** **T**oroidal **L**HC **A**pparatu**S** draws the attention to the particular form of the ATLAS magnets.

A thick coat of the toroidal 4 T magnetic field surrounds inner layers of the detector system: hadron and electromagnetic calorimeters and inner tracking detectors. This field is provided by the set of super-conductive coils which is schematically shown[1] in Fig. 1. A small cylinder in the center of the system indicates the central solenoid, described below.

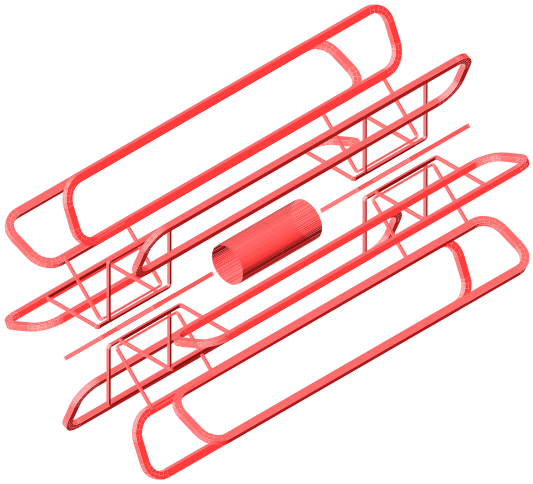

Fig. 1. 3-Dimensional view of the bare winding of the ATLAS Magnet System: the Central Solenoid, the 8 coils of the Barrel Toroid and 2 x 8 coils of the End-Cap Toroids.

2.1. Magnets

The ATLAS Magnet System consists of

- the air-core barrel toroid
- two air-cored end-cap toroids
- the central solenoid

The barrel toroid as well as each of two end-cap toroids consists of 8 coils. Their relative positions are shown in Fig. 2. All coils of barrel and end-cap toroids are air core super-conducting magnets normally operating

[1] Majority of figures shown in this note come from ATLAS Collaboration Technical Design Reports listed in the bibliography

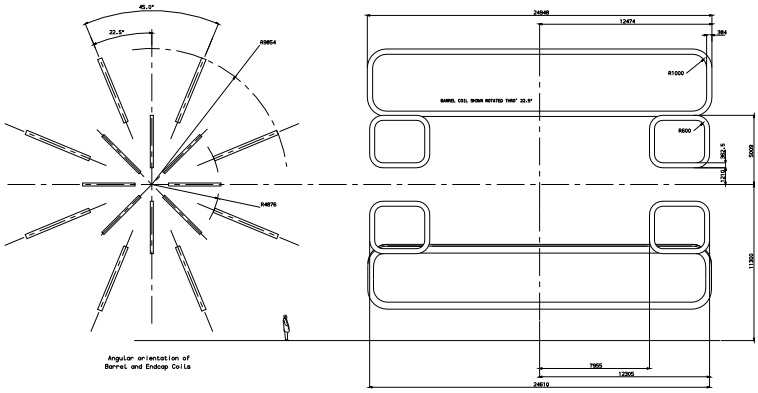

Fig. 2. Side and longitudinal view of the toroids showing their spatial positions.

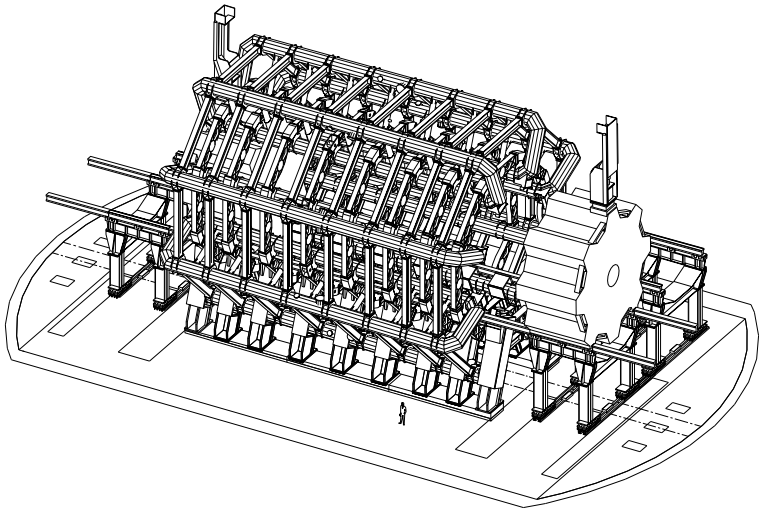

Fig. 3. Three-dimensional view of the super-conducting air-core toroid magnet system. The right-hand end-cap magnet is shown retracted from its operating condition.

at 4.5^0K. Detailed informations on the fabrication of super-conductive coils, on cryogenics, refrigeration plant, magnet power system and control can be found in series of the ATLAS Collaboration Technical Design Reports [5–7].

The barrel toroid coils have individual cryostats taking up forces between coils. Eight end-cap coils are assembled and housed in one large cryostat. Note the overlap in radial direction leading to the corrugated shape of the end-cap toroid cryostats seen on Fig. 3

The toroidal structure is then built up with 8 cryostats and various linking elements providing mechanical stability. These stiffeners, struts, voussoirs and pillars have to carry not only the self-weight of the magnet system but — in fact the main component — enormous magnetic forces which tend to deform the structure. For information about the scale: the compressive force between Barrel and End-Cap Toroids is 240 tons per End-Cap. Stress levels and deformations in the structure are studied in great details taking into an account not only normal conditions but also exceptional loads which may come e.g from a seismic acceleration, magnetic fault of one of the eight coils etc. It is assumed that the maximum deformation should not exceed 20 mm. Taking the dimensions of the System summarized in Table I one obviously adds this construction to the long list of ATLAS challenging tasks.

Another characteristic solution of the ATLAS magnet system is superconducting central solenoid. It is placed inside calorimeters. Such position of the solenoid in front of the electromagnetic calorimeter required the minimization of the material. In consequence, the solenoid is housed in the liquid argon calorimeter cryostat and the coil is designed to be as thin as

TABLE I

Main parameters and operating conditions of the magnet system

	Units	Barrel Toroid	2 End-Cap Toroids	Central Solenoid
No. of coils		8	2 x 8	1
Inner diameter	m	9.4	1.65	2.44
Outer diameter	m	20.1	10.7	2.63
Axial length	m	25.3	5	5.3
No. of turns per coil		120	116	1173
Nominal Current	kA	20.5	20	8
Ampere-turns	MAt	19.68	18.5	9.4
Peak field	T	3.9	4.1	2.6
Circuit resistance	mΩ	0.160	0.244	0.413
Inductance	H	5.5	2.0	1.3
Current ramp rate	A/s	2.3	5.6	5.0
Ramp-up time	minutes	135	60	30
Max dI/dt	A/s	8	5.5	6
Run-down time	minutes	130	140	30
Fast discharge time	s	77	37	29
Stored energy	MJ	1080	410	39
Cold mass	tons	365	214	5.5

possible without sacrifying the reliability and safety. In effect the solenoid contributes to the material budget less than 1 X_0 at normal incidence. It provides 2 T field in space filled by the ATLAS inner detector. Iron of the hadron calorimeter serves as the return yoke for this field.

2.2. System performance

The performance of the toroid magnet system in terms of bending power is characterized by the $\int Bdl$, field integral where B is the azimuthal field component and dl is taken over the straight line trajectory between the inner and outer radius of the toroids. The field integral is function of the pseudorapidity and depends also on the initial azimuthal angle as the field density has certain angular structure. Such structure is illustrated in Fig. 4 where magnetic field map is shown for the plane normal to the beam axis, in the middle of the end-cap toroid.

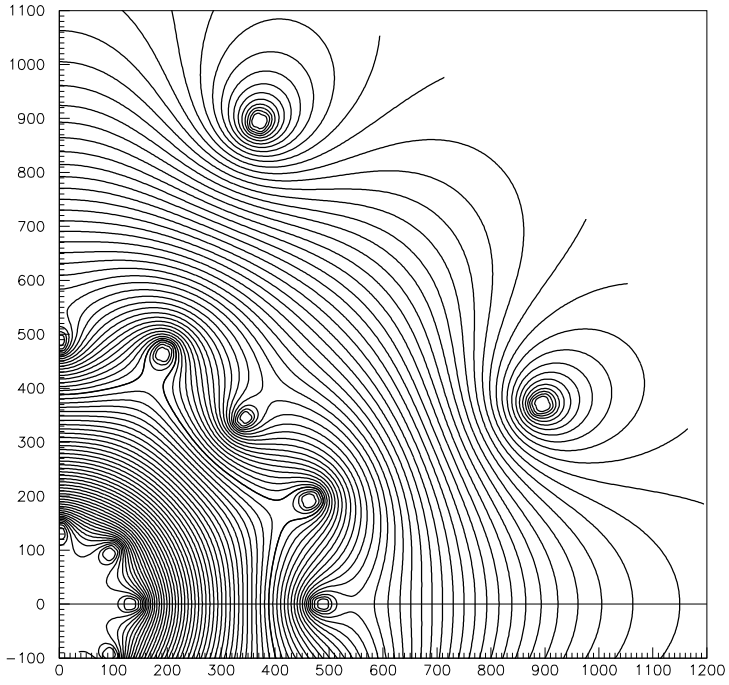

Fig. 4. Magnetic field map in the transition region. The field lines are shown in a plane perpendicular to the beam axis and located in the middle of the end-cap toroid. The interval separating consecutive lines is 0.1 Tm. Individual barrel and end-cap coils are visible. The scales are in centimeters.

The field integral values for pseudorapidities from the range 0–2.7 and for azimuthal angles in range 0–$\pi/8$ are shown in Fig. 5. The barrel toroid ($0 < \eta < 1.3$) provides 2–6 Tm while in the region of end-cap toroids field integrals are 4–8 Tm. These calculations are still simplified. For the reconstruction of real particle trajectories with full precision the influence of the solenoid field and magnetized iron of hadron calorimeters has to be included as well as details of the muon chamber layout.

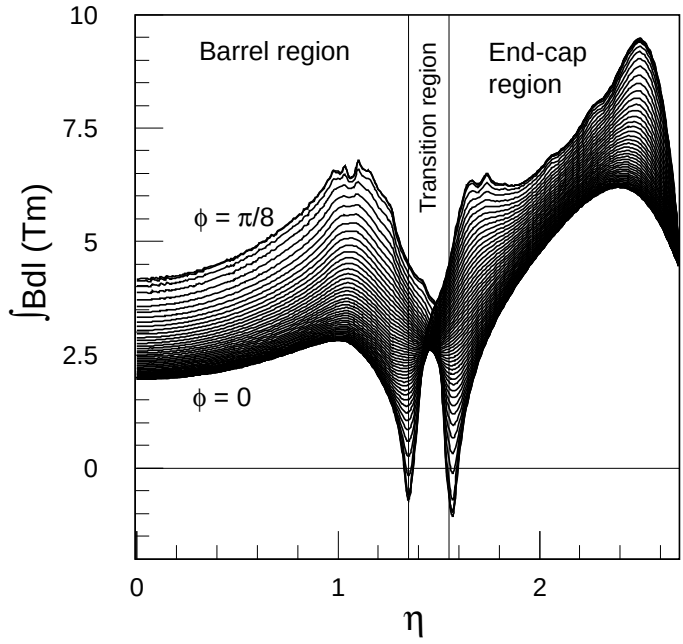

Fig. 5. Field integrals vs pseudorapidity η.

The toroid magnet system and sets of muon chambers form the ATLAS muon spectrometer which provides fast muon triggers and serves as precision muon tracker. This is sketched on Fig. 6 which also shows geometrical proportions of the muon spectrometer, calorimetry (shaded areas) and the inner detector region.

Many different effects contribute to the momentum resolution of the muon spectrometer. At high momentum (p_{T} above 300 GeV) the intrinsic detector precision dominates the resolution. At the range of $30 < p_{\mathrm{T}} < 300$ GeV the resolution is limited by multiple scattering while at low momentum, below 30 GeV, energy loss become dominant, particularly in central region of the detector. This is shown in more details on Fig. 7

Measurements of multi-muon final states are essential for many new searches. The mass resolutions and reconstruction efficiencies of the muon

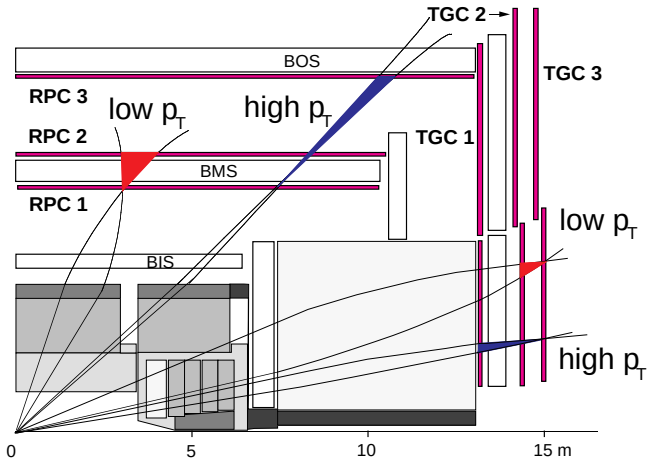

Fig. 6. The LVL1 muon trigger scheme in the barrel and in the end-cap. The low-p_T trigger is based on two double layers of trigger chambers; the high-p_T trigger uses an additional double layer in the barrel and a triple layer in the end-cap. The shaded area represents the calorimeters and the absorber. Trajectories for positive and negative muons are shown.

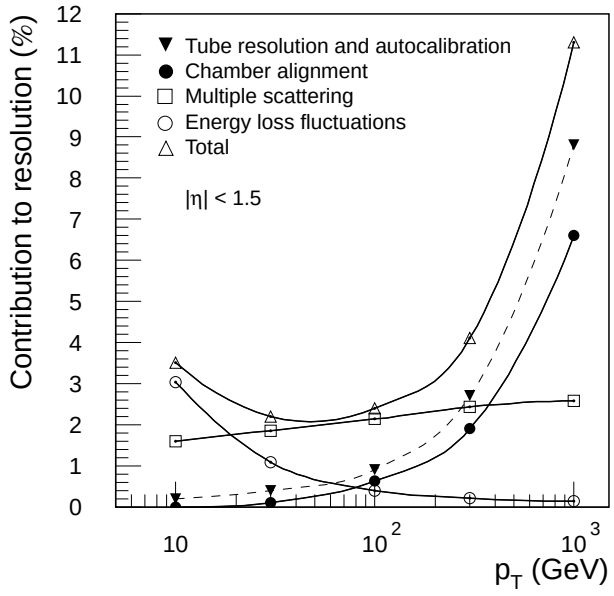

Fig. 7. Contributions to the momentum resolution in the muon spectrometer, averaged over $|\eta| < 1.5$.

spectrometer were carefully evaluated with full detector simulation and reconstruction for a sample of selected benchmark processes [4] ($W'^{\pm} \to \mu^{\pm} + X$ for single muon final states; dimuon final states were generated in MSSM process $A^0 \to \mu^+\mu^-$ for $M_{\mu\mu} < 800$GeV, and the Extended Gauge Model process $Z' \to \mu^+\mu^-$ for $M_{\mu\mu} > 800$GeV.

For the four muon final states results come from the extensive studies of the decay process $H^0 \to ZZ \to \mu^+\mu^-\mu^+\mu^-$. Here, the typical reconstruction efficiencies are ~88% when the geometrical acceptance for single muon is 97%. Four-muon invariant mass is reconstructed with resolution which ranges from 1.8% to 2.6% for the mass range of 100 to 800 GeV.

The reconstruction efficiency for dimuon final states is typically 93% in the wide range of $M_{\mu\mu}$ from 100 to 1000 GeV. The reconstructed mass resolution shows certain dependence on the reconstructed mass above 800 GeV. It ranges from 2.4% to 3.4% below 800 GeV and from 4.2% to 13% for higher masses (1 TeV–5 TeV).

Clean identification of muon charges is another essential feature for many physics topics. Results of present studies show that the probability of the muon charge misidentification is in the range of 0.2% to 0.9% for a W' of 1TeV and does not exceeds 4% for W' of 6 TeV ($W'^{\pm} \to \mu^{\pm}\nu$ events were used for these studies). More detailed results are reported recently in [1].

3. Transition Radiation Tracker

The Transition Radiation Tracker is undoubtfuly another distinctive element of the ATLAS detector system. Recently, one observes an increasing number of experiments using transition radiation detectors. But the geometrical scale, more than 400 000 electronics channels and heavy radiation environment makes the ATLAS TRT construction exceptional.

Transition radiation effect has been described by Frank and Ginzburg in 1946 [9]. When a charged relativistic particle passes boundary of materials of different dielectric constants it emits an electromagnetic radiation with certain frequency range and angular distribution, narrow and peaked in forward direction. The effect depends on γ of the particle and it was early realized that it may serve for particle (mass) identifications at high energies. Nevertheless, about 35 years passed before developments of experimental concepts and technology allowed for the first successful applications. I believe that the important breakthrough came only in 1981 with the proposition [10] to detect TR by counting rates of energy clusters above few keV in relation to the low energy ionisation depositions. Certain material and detector optimizations allow to limit the small but significant background coming from the δ electrons.

In practical realizations TR detector consists of repeating structure: radiator-detector, where radiator provides numerous material transitions and detector ("classical", often gas chambers) should efficiently respond both, to the low energy ionisation depositions and to the energetic clusters ($\sim$ 5 keV), characteristic for the transition radiation.

3.1. Continuous tracking and electron-pion identification

In ATLAS detector TRT serves two functions. It provides many coordinate measurements for tracks of charged particles passing through the detecting elements, straws. These straws are gas drift narrow tubes 4mm in diameter. The gas mixture (70% Xe + 20% CF_4 + 10% CO_2) is selected for the good efficiency in TR cluster absorption. Every tube is equipped with the readout electronics which allows to measure the distance from a track to the central anode wire by measuring the time it takes electrons created along the track to drift in to the central wire. The electronics is also able to record low threshold (200 eV) crossings corresponding to the minimum ionizing passages as well as high threshold crosses of 5 keV corresponding to the transition radiation candidates.

Proper understanding of detector response required careful simulations and prototype measurements. Measurements and model calculations of energy depositions by high energy pions an electrons are shown in Fig. 8. Comparison of this distributions for pions and electrons shows a significant tail for electrons at high depositions, coming from TR photons.

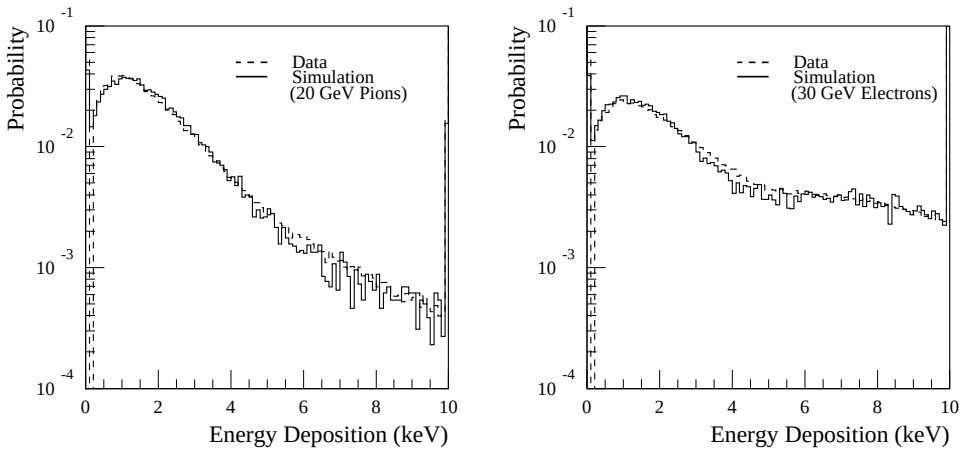

Fig. 8. Ionisation energy deposition collected on a straw from pions with $p_{\mathrm{T}} = 20$ GeV (left) and combined ionisation and TR energy deposition collected on a straw from electrons with $p_{\mathrm{T}} = 30$ GeV (right).

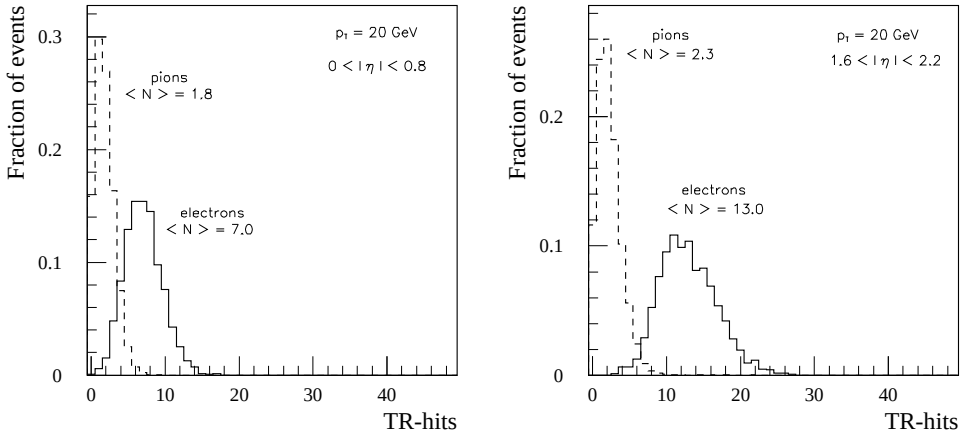

Fig. 9. Number of TR hits for electron and pions with $p_{\mathrm{T}} = 20$ GeV and $0 < |\eta| < 0.8$ (left) and $1.6 < |\eta| < 2.2$ (right).

Another manifestation of the TR performance of the ATLAS TRT are simulation results shown in Fig. 9. The identification efficiency is determined by the size of the overlapping region and is often expressed by the pion rejection (the reciprocal of the efficiency) for a chosen electron efficiency of 90%.

TRT detector Fig. 10 has barrel section which contains about 50 000 straws, each divided at the center to reduce the occupancy and read out at each end. The end-caps contain 320 000 straws. The total number of electronics channels is 420 000.

The barrel straws are assembled in modules containing from 329 to 793 axially oriented straws. Barrel modules cover radial range from 56 to 107 cm. High occupancy of straws in the six innermost layers is reduced by making its central 80 cm inactive.

The two end-caps consist of 18 wheels with radial straws. The 14 central wheels cover the radial range from 64 to 103 cm. The outer four wheels extend to an inner radius of 48 cm. The wheels 7 to 14 have half as many straws per cm in z (beam) direction as other wheels to maintain constant number of hits per track over whole rapidity range. This is one principal concepts of the ATLAS inner detector layout.

Many detailed physics simulations have shown that combination of precision tracking provided by pixel and micro-strip detectors and continuous tracking in TRT is very robust. Also electron identification is a valuable tool for physics [11, 1].

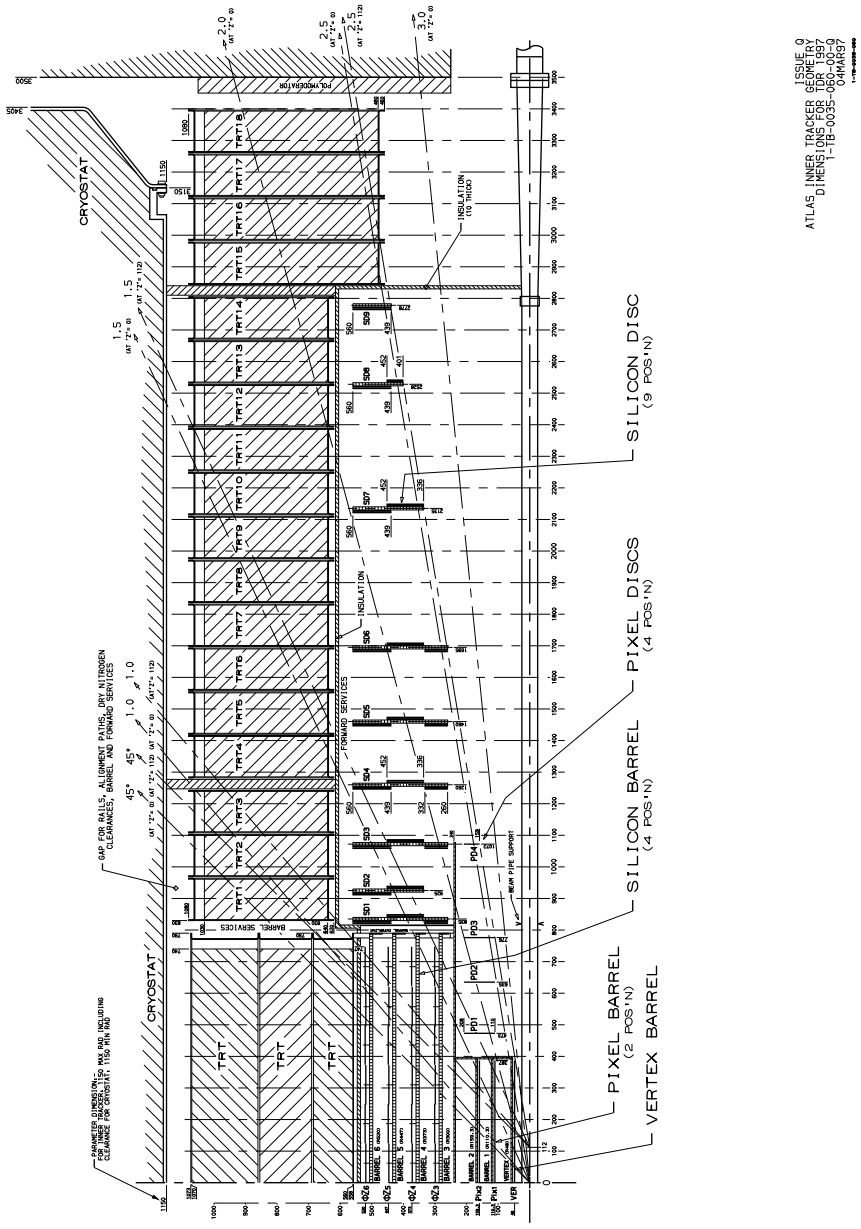

Fig. 10. Inner detector layout. A cross-section of the Inner Detector engineering layout through the beam axis.

REFERENCES

[1] Detector and Physics Technical Design Report, CERN/LHCC/99-14/15, May 1999.

[2] E. Richter-Wąs, *Acta Phys. Pol.* **B30**, 3933 (1999), this Proceedings.

[3] F. Gianotti, Precision Physics at LHC. IV-th International Symposium on Radiative Corrections, Barcelona, September, 1998.

[4] ATLAS Muon Spectrometer Technical Design Report, CERN/LHCC/97-22, ATLAS TDR 10, 31 May, 1997.

[5] ATLAS Magnet System Technical Design Report, CERN/LHCC/97-18 ATLAS TDR 6, 30 April, 1997.

[6] ATLAS Barrel Toroid Technical Design Report, CERN/LHCC/97-19, ATLAS TDR 7, 30 April, 1997.

[7] ATLAS End-Cap Toroids Technical Design Report, CERN/LHCC/97-20, ATLAS TDR 8, 30 April, 1997.

[8] ATLAS Central Solenoid Technical Design Report, CERN/LHCC/97-21, ATLAS TDR 9, 30 April, 1997.

[9] V.L. Ginzburg, I.M. Frank, *Zh. Eksp. Teor. Fiz.* **16**, 15 (1946).

[10] T. Ludlam *et al.*, *Nucl. Instrum. Methods* **180**, 431 (1981).

[11] ATLAS Inner Detector Technical Design Report, CERN/LHCC/97-4/5 ATLAS TDR 4 and 5, 30 April, 1997